Multifrequency third-harmonic generation by red-shifting solitons in a multimode photonic-crystal fiber

A. B. Fedotov,[1,2] A. A. Voronin,[1] E. E. Serebryannikov,[1] I. V. Fedotov,[1] A. V. Mitrofanov,[1] A. A. Ivanov,[2,3] D. A. Sidorov-Biryukov,[2] and A. M. Zheltikov[1,2]

[1]*Department of Physics, M. V. Lomonosov Moscow State University, Vorob'evy gory, Moscow 119992, Russia*

[2]*International Laser Center, M. V. Lomonosov Moscow State University, Vorob'evy gory, Moscow 119992, Russia*

[3]*Center of Photochemistry, Russian Academy of Sciences, ulica Novatorov 7a, Moscow 117421, Russia*

(Received 17 May 2006; revised manuscript received 14 September 2006; published 25 January 2007)

While the standard scenario of third-harmonic generation (THG) by a dispersive-wave pump involves the emission of light with a frequency 3ω, thrice the frequency ω of the input pump field, solitons undergoing a continuous shift of their central frequency ω due to the Raman effect in a multimode optical fiber can generate the third harmonic in a different fashion. In the experiments reported here, we provide the first direct experimental evidence of THG by a continuously red-shifting soliton pump by studying the third-harmonic buildup in relation to the spectral evolution of the soliton pump field in a silica photonic-crystal fiber (PCF). We show that solitons excited in a PCF by unamplified femtosecond pulses of a Cr:forsterite laser sweep through the spectral range from 1.25 to 1.63 μm, scanning through a manifold of THG phase-matching resonances with 3ω dispersive waves in PCF modes. As a result, intense third-harmonic peaks build up in the range of wavelengths from 370 to 550 nm at the output of the fiber, making PCF a convenient fiber-format multifrequency source of short-wavelength radiation. Time-resolved fluorescence measurements with photoexcitation provided by the third-harmonic PCF output are presented, demonstrating the high potential of PCF sources for an ultrafast photoexcitation of fluorescent molecular systems in physics, chemistry, and biology.

DOI: 10.1103/PhysRevE.75.016614 PACS number(s): 42.65.Wi

I. INTRODUCTION

Third-harmonic generation (THG) is one of the basic nonlinear-optical processes which has been intensely studied since the early days of nonlinear optics [1,2]. This process has been widely used [3] to generate short-wavelength radiation for high-resolution imaging, spectroscopy, microfabrication, direct excitation of electronic molecular transitions, multiphoton ionization, stimulation, and steering of photochemical and photobiological processes, as well as preparation of vibrational wave packets [4]. Standard THG strategies involve cascading second-order nonlinear-optical processes phase-matched by crystal anisotropy [1,2] or periodic poling in crystals with a high quadratic nonlinearity [5].

The advent of photonic-crystal fibers (PCFs) [6,7] has opened a new phase in nonlinear optics, offering new solutions for the creation of compact and efficient fiber-optic light sources [8,9] and optical frequency converters [10]. Controlled dispersion of guided modes [11] and large interaction lengths [9] provided by these fibers for light fields strongly confined in a small fiber core [12,13] result in a radical enhancement of nonlinear-optical frequency conversion and spectral transformation of laser radiation. Third-order nonlinear-optical processes enhanced in PCFs now offer a useful fiber-format alternative to frequency-conversion cascades using $\chi^{(2)}$ nonlinear crystals [14]. Highly efficient THG has been recently observed in fused silica [15–21] and multicomponent-glass PCFs [22,23], as well as in tapered fibers [24]. THG-based PCF sources of short-wavelength radiation have been recently shown [25] to be a convenient and powerful tool for time-resolved fluorescence studies on a broad class of organic molecules.

Femtosecond laser pulses propagating in the range of anomalous dispersion in PCFs tend to couple into solitons [26]. Due to the retarded optical nonlinearity of a fiber material, solitons undergo a continuous frequency downshift as they propagate through a fiber, a phenomenon known as soliton self-frequency shift (SSFS) [27,28]. PCFs with a high optical nonlinearity can substantially enhance this effect [29], allowing the creation of efficient and compact fiber-format frequency shifters for spectroscopy and imaging [30–32] and suggesting a convenient pump-seed synchronization scheme in optical parametric chirped-pulse amplification [33]. Red-shifted solitons can also serve as a pump for THG [20,23]. Since dispersion of solitons differs from the dispersion of linear dispersive waves existing at the same frequency in a material or a waveguide structure, phase-matching conditions for a THG process with a soliton pump are not reduced to the standard phase-matching condition for THG with a dispersive-wave pump field [23]. The nondispersive nature of solitons, as shown in earlier work [34,35], modifies phase matching for four-wave mixing (FWM) involving solitons and linear dispersive waves relative to conventional FWM involving only dispersive waves. Experimental observation of FWM involving both solitons and dispersive waves has been reported by Efimov *et al.* [36]. In a recent experiment [23], THG by a soliton pump has been observed.

While the earlier studies have shown the possibility of frequency up-conversion to the short-wavelength region through THG in high-order modes of PCFs [15–19], revealed the physical mechanisms shifting the central frequency of the third harmonic from 3ω [14,21], and demonstrated new phase-matching options in dispersive-wave THG by a soliton pump [23], in this work we analyze the buildup of the third-harmonic signal in relation to the spectral evolution of the soliton pump field in a PCF to provide direct experimental

evidence of THG by a continuously red-shifting soliton pump. We will show that while standard THG scenarios involve the emission of light with a frequency 3ω, thrice the frequency ω of the input pump field, solitons undergoing a continuous shift of their central frequency ω due to the Raman effect in a multimode optical fiber can generate the third harmonic in a different fashion. In the experiments reported here, solitons excited in a PCF by unamplified 100–120-fs pulses of a Cr:forsterite laser sweep through the spectral range from 1.25 to 1.63 μm, scanning through a manifold of THG phase-matching resonances with 3ω dispersive waves in PCF modes. As a result, intense third-harmonic peaks build up in the range of wavelengths from 370 to 550 nm at the output of the fiber, making PCF a multifrequency source of short-wavelength radiation.

II. PROPAGATION DYNAMICS OF ULTRASHORT LASER PULSES IN GUIDED MODES OF PHOTONIC-CRYSTAL FIBERS

To explore the dynamics of laser pulses propagating through the PCF, we numerically solved the generalized nonlinear Schrödinger equation (GNSE) [26,37] for the field envelope $A=A(z,t)$:

$$\frac{\partial A}{\partial \xi} = -\frac{\alpha^{(0)}}{2}A - i\frac{\alpha^{(1)}}{2}\frac{\partial A}{\partial \tau} + i\sum_{k=2}^{6}\frac{(i)^k}{k!}\left(\beta^{(k)} + i\frac{\alpha^{(k)}}{2}\right)\frac{\partial^k A}{\partial \tau^k} + P_{nl}(\xi,\tau), \quad (1)$$

where z is the propagation coordinate, t is the time variable, τ is the retarded time, $\beta^{(k)}=\mathrm{Re}[\partial^k\beta/\partial\omega^k]$, and β is the propagation constant of the waveguide mode. Fiber losses are included through the coefficients $\alpha^{(k)}=\mathrm{Im}[\partial^k\beta/\partial\omega^k]$. The nonlinear polarization $P_{\mathrm{nl}}(\xi,\tau)$ in Eq. (1) is defined in such a way [38] as to include the retarded nonlinearity of the fiber material and the wavelength dependence of the effective mode area:

$$P_{nl}(\xi,\tau) = i\hat{F}^{-1}\left[\frac{n_2\omega}{cS_{eff}(\omega)}\tilde{p}_{nl}(\xi,\omega_0-\omega)\right], \quad (2)$$

where n_2 is the nonlinear refractive index of the fiber material, ω is the current frequency, ω_0 is the central frequency of the input field, c is the speed of light, $S_{eff}=[\int_{-\infty}^{\infty}\int_{-\infty}^{\infty}|f(x,y)|^2dxdy]^2/\int_{-\infty}^{\infty}\int_{-\infty}^{\infty}|f(x,y)|^4dxdy$ is the effective mode area, $f(x,y)$ is the field profile in a waveguide mode, and the operator $\hat{F}^{-1}(\bullet)$ denotes the inverse Fourier transform. The frequency-domain nonlinear polarization in Eq. (2) is defined through the direct Fourier transform,

$$\tilde{p}_{nl}(\xi,\omega-\omega_0) = \hat{F}\left[A(\xi,\tau)\int_{-\infty}^{\infty}R(t)|A(\xi,\tau-t)|^2dt\right], \quad (3)$$

including both the instantaneous, Kerr nonlinearity and the retarded, Raman contribution via the nonlinear response function

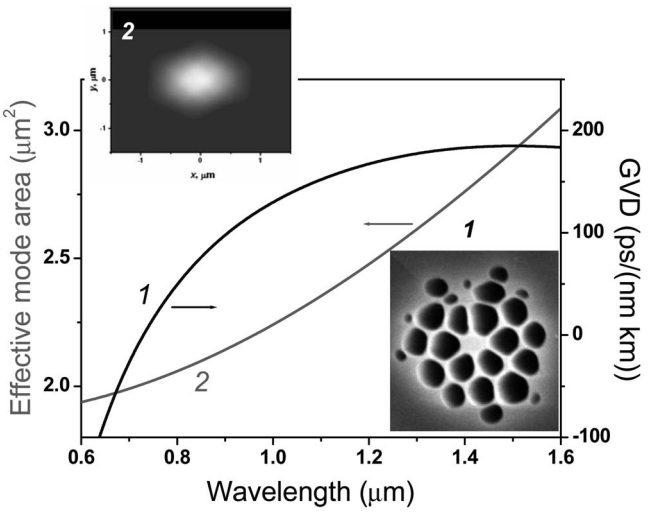

FIG. 1. Group-velocity dispersion (curve 1) and the effective mode area S_{eff} (curve 1) calculated as functions of radiation wavelength for the fundamental mode of the PCF shown in inset 1. Inset 2 displays the transverse field intensity profile in the fundamental PCF mode.

$$R(t) = (1-f_R)\delta(t) + f_R\Theta(t)\frac{\tau_1^2+\tau_2^2}{\tau_1\tau_2^2}e^{-t/t_2}\sin\left(\frac{t}{\tau_1}\right), \quad (4)$$

where f_{R} is the fractional contribution of the Raman response; $\delta(t)$ and $\Theta(t)$ are the delta and the Heaviside step functions, respectively; and τ_1 and τ_2 are the characteristic times of the Raman response of the fiber material. For fused silica, $f_{\mathrm{R}}=0.18$, $\tau_1=12.5$ fs, and $\tau_2=32$ fs. The nonlinear polarization $P_{\mathrm{nl}}(\xi,\tau)$ defined in the form of Eq. (2) not only helps to include the influence of the frequency-dependent effective mode area S_{eff} on the nonlinear coefficient $\gamma=(n_2\omega)/(cS_{\mathrm{eff}})$, but also gives a correct definition of the local field intensity, which also depends on $S_{\mathrm{eff}}(\omega)$.

In experiments presented below in this paper, we used a silica PCF with a cross-section structure shown in inset 1 to Fig. 1 and a core diameter of 1.85 μm. To analyze dispersion properties and transverse field profiles $f(x,y)$ for the guided modes of this type of PCF, we employed a numerical procedure based on polynomial expansion in localized functions [39]. Figure 1 displays the group-velocity dispersion (GVD) and the effective mode area S_{eff} calculated as functions of radiation wavelength for the fundamental PCF mode (shown in inset 2 in Fig. 1). The GVD for the fundamental PCF mode vanishes at 730 nm (curve 1), providing anomalous regime of pulse propagation for 1.25-μm radiation of Cr:forsterite laser. Effective mode area S_{eff} tends to increase for longer wavelengths (curve 2) because of diffraction, leading to a lower nonlinearity of the PCF in the long-wavelength range. At the central wavelength of Cr:forsterite laser radiation (1.25 μm), the effective mode area of the fundamental PCF mode is 2.5 $\mu\mathrm{m}^2$, which corresponds to the nonlinear coefficient $\gamma\approx 60$ $(\mathrm{km\ W})^{-1}$.

Cr:forsterite laser radiation is red-shifted in our experiments through soliton mechanisms, generating the third harmonic in the range of wavelengths from 370 to 550 nm. In

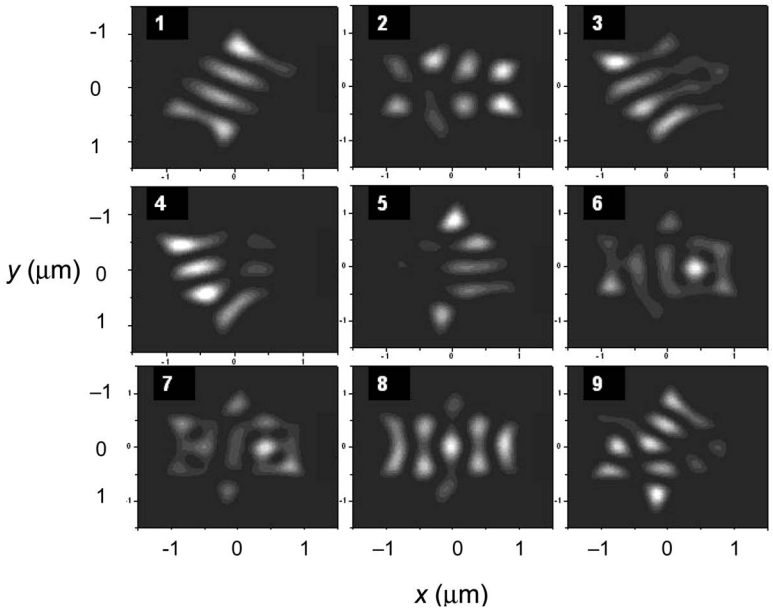

FIG. 2. High-order PCF modes allowing phase matching between a dispersive-wave third-harmonic field and solitons excited by Cr:forsterite laser pulses in the fundamental PCF mode.

this range, the considered type of PCF is essentially multimode. High-order waveguide modes play a significant role in the THG process, as they provide phase matching between the red-shifted solitons and dispersive-wave third-harmonic field. For a given fiber dispersion profile, such a phase matching is impossible for the third harmonic generated in the fundamental mode, which is quite typical of THG in optical fibers. In Fig. 2, we present field intensity profiles for nine high-order guided modes of the considered type of PCF that contribute to the multimode-phase-matched THG process in our experiments.

III. EXPERIMENTAL RESULTS AND DISCUSSION

A. Soliton dynamics of femtosecond pump pulses

In experiments, we used a Cr:forsterite laser system based on a two-arm long-cavity master oscillator consisting of a 10-mm Cr^{4+}:forsterite crystal, a set of totally reflecting mirrors, an 8% output coupler, and a prism pair for dispersion compensation. The laser oscillator was pumped with a 7.5-W ytterbium fiber laser radiation. The laser cavity was adjusted to generate 70–120-fs pulses with an average power up to 180 mW and a central wavelength of 1.25 μm at a repetition rate of about 20 MHz.

Cr:forsterite laser pulses tend to form optical solitons as they propagate through the PCF in the regime of anomalous dispersion. These solitons experience a continuous frequency downshift due to the Raman effect. In Fig. 3, we present a characteristic example of efficient soliton frequency shifting of an unamplified Cr:forsterite laser pulse with an initial energy of 0.5 nJ and an input spectrum shown by the dashed line. The input pulse is efficiently coupled into a soliton, which experiences a wavelength shift exceeding 100 nm within 12 cm of PCF due to the Raman effect.

The soliton wavelength shift increases as the solitons propagate along the fiber (Fig. 4). Group-delay effects transfer this spectral shift into the time delay of solitons, leading to the isolation of frequency-shifted solitons in the time domain. For a short (3-cm) piece of PCF, wavelength-shifted solitons still partially overlap in time and frequency, which gives rise, as can be seen from the upper panel in Fig. 4, to well-pronounced interference fringes in the long-wavelength part of the output spectrum. As the radiation field propagates further on along the fiber, the frequency separation and the time interval between the red-shifted solitonic peaks increase (the upper panel in Fig. 4). As a result, for longer pieces of PCF, frequency-shifted solitons are observed as well-resolved peaks in the long-wavelength part of the output spectra (spectral peaks centered at 1.44 and 1.59 μm for a 30-cm PCF in Fig. 4). As can be seen from the comparison of the experimental spectra (filled circles in Fig. 4) with the results of numerical simulations (the solid line in Fig. 4), the GNSE-based model, defined by Eqs. (1)–(4), provides an adequate description of the main tendencies in the spectral transformation of Cr:forsterite laser pulses in PCFs observed

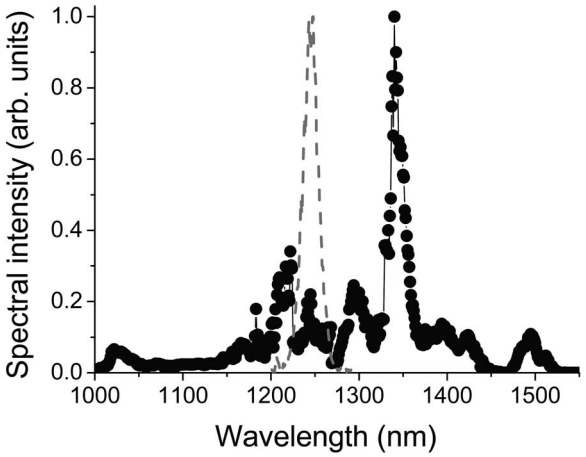

FIG. 3. The spectrum of Cr:forsterite laser pulses transmitted through a 12-cm PCF (filled circles connected by a solid line). The spectrum of the input pulse is shown by the dashed line. The input pulse energy is 0.5 nJ.

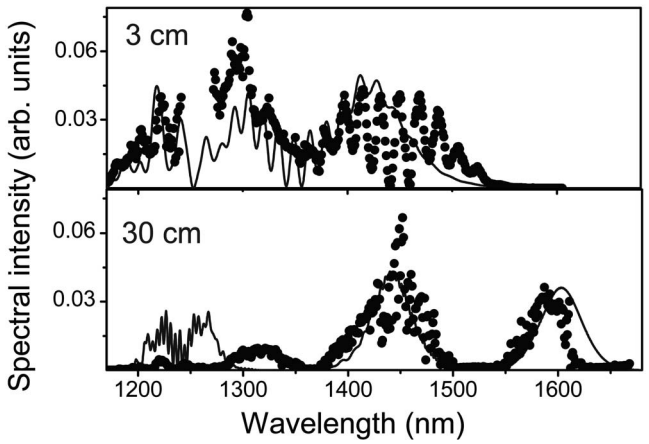

FIG. 4. Measured (filled circles) and computed (solid line) spectra of Cr:forsterite laser pulses transmitted through the PCF with a length of 3 cm (upper panel) and 30 cm (lower panel). The input pulse energy is 1.2 nJ. The initial pulse width is 120 fs.

in our experiments. High-order dispersion and the wavelength dependence of the effective mode area (Fig. 1) tend to reduce the SSFS rate in the long-wavelength spectral region (see also [40,41]).

B. Third-harmonic generation by frequency-shifting solitons

The third harmonic is generated in PCFs by laser radiation of any wavelength lying within the fiber transmission range through the third-order optical nonlinearity of fiber material. However, the efficiency of THG becomes sufficient to yield an intense signal in the spectrum at the output of the fiber only if the phase-matching condition is satisfied. In standard regimes of THG in a bulk material or in a waveguide [1,2], pump radiation with a given spectrum centered at frequency ω generates the third-harmonic signal centered at 3ω. Phase matching then requires the equality of refractive indices (effective mode indices in waveguide THG) at the pump and third-harmonic frequencies,

$$n_m(3\omega) = n_n(\omega), \tag{5}$$

where $n_m(3\omega)$ and $n_n(\omega)$ are the effective mode indices, which can include both waveguide and material dispersion for the mth and nth waveguide modes at the frequencies of the third harmonic and the pump field, respectively.

In the case considered here, frequency-shifting solitons serve as a pump field. The central frequency of the pump ω is thus a variable which changes as a function of the propagation coordinate. In this regime, the pump field with a constantly varying central frequency sweeps over a broad wavelength range (from 1250 to 1630 nm in our experiments, see Figs. 3 and 4, and inset 2 in Fig. 5), allowing the generation of the third harmonic at different frequencies 3ω. Phase matching, however, allows efficient THG only at those frequencies where the soliton pump is phase-matched with the dispersive-wave third-harmonic field. This type of phase matching physically and mathematically differs from phase matching for THG with a dispersive-wave pump.

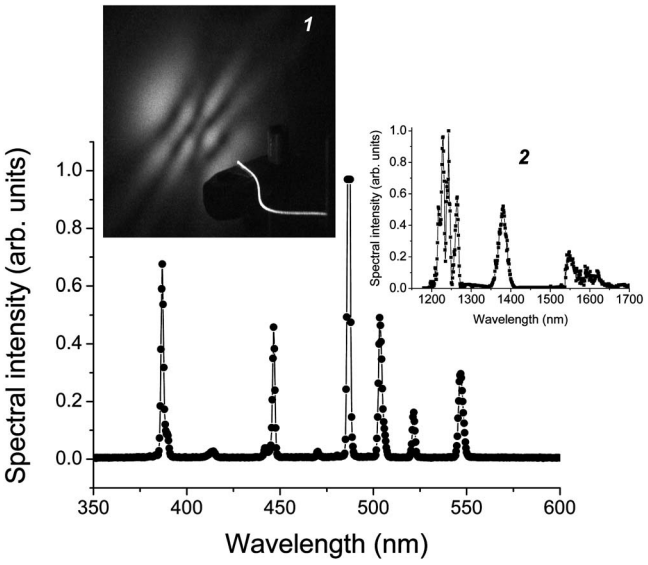

FIG. 5. Typical spectrum of the third-harmonic PCF output. The fiber length is 35 cm. The input pulse energy is 2.5 nJ. The initial pulse width is 100 fs. Inset 1 shows the far-field image of the third-harmonic beam from the PCF. Inset 2 displays the infrared part of the PCF output spectrum under the same experimental conditions.

To analyze phase matching for a THG process where a soliton pump field generates dispersive-wave third harmonic through the cubic nonlinearity of the medium, we represent the electric field in the soliton as

$$A = \psi(\xi)\exp\{-i\omega_s t + i[\beta_n(\omega_s) + q]z\}, \tag{6}$$

where $\xi = t - z/v_g$ is the retarded time, β_n is the propagation constant of the nth waveguide mode, z is the propagation coordinate, ω_s and v_g are the central frequency and the group velocity of the soliton, $\psi(\xi)$ is the soliton pulse shape, $q = \gamma P/2$, and P is the soliton peak power.

Representing A in Eq. (6) in the form of a Fourier integral,

$$A = \int \hat{F}(\omega)\exp\left\{-i(\omega_s - \omega)t + i\left[\beta_n(\omega_s) + q - \frac{\omega_s - \omega}{v_g}\right]z\right\}d\omega, \tag{7}$$

where $\hat{F}(\omega)$ is the Fourier transform of the soliton spectrum, we introduce the soliton propagation constant (see also [42,43])

$$\beta_{sol}(\omega) = \beta_n(\omega_s) + q + \frac{\omega - \omega_s}{v_g}. \tag{8}$$

The propagation constant of dispersive-wave third harmonic emitted in the mth guided mode is written as

$$\beta_{TH}(3\omega) = \beta_m(3\omega). \tag{9}$$

With the effective mode index for the dispersive-wave third harmonic defined as $n_m(3\omega) = \beta_{TH}(3\omega)c/(3\omega)$, the phase-matching condition for THG by a soliton pump field is given by

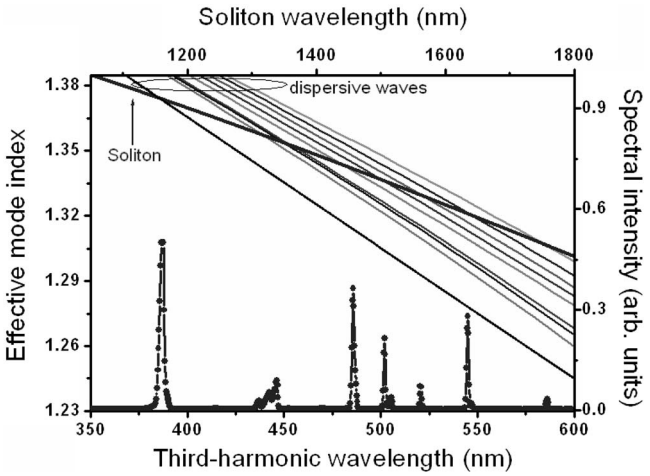

FIG. 6. Spectrum of the third harmonic (filled circles connected by a solid line) generated in a 30-cm PCF by 2-nJ 120-fs Cr:forsterite laser pulses. Solid lines labeled as dispersive waves show the effective mode indices n_m of high-order PCF modes with field intensity profiles presented in Fig. 2 as functions of radiation wavelength in the short-wavelength (third-harmonic) spectral range (the lower abscissa axis). The bold line shows the effective mode index n_{sol} of the soliton pump in the fundamental PCF mode as a function of the pump wavelength (the upper abscissa axis). Phase matching is achieved at the wavelengths λ where the bold line, representing $n_{\mathrm{sol}}(\lambda)$, crosses one of the solid lines, representing $n_m(\lambda/3)$.

$$n_m(3\omega) = n_{\mathrm{sol}}(\omega), \tag{10}$$

where $n_{\mathrm{sol}}(\omega)=\beta_{\mathrm{sol}}(\omega)/k$ is the effective mode index for the soliton, $k=2\pi/\lambda$, and λ is the radiation wavelength.

Equality (10) illustrates our argument that the phase-matching condition for THG with a soliton pump differs from the phase-matching condition for THG with a dispersive-wave pump [Eq. (5)]. The nonlinear nature of a soliton pump modifies its dispersion relative to a linear dispersive wave through the nonlinear term q in Eq. (8). Phase matching under these conditions becomes dependent on the peak power of the pump field.

In Fig. 5, we present a typical spectrum of the third harmonic generated in the considered type of PCF by 100-fs 2.5-nJ Cr:forsterite laser pulses. The spectrum of the third harmonic produced under these conditions features a set of intense peaks with wavelengths ranging from 370 to 550 nm. The far-field beam pattern of the third-harmonic signal indicates that the third harmonic is most efficiently generated in high-order PCF modes (cf. Fig. 2 with inset 1 in Fig. 5). Well-resolved peaks observed in the infrared part of the PCF output spectrum (inset 2 in Fig. 5) visualize the red-shifted solitons produced by input laser pulses. The spectrum of the solitonic part of the field propagating in the fiber stretches up to 1.63 μm.

In Fig. 6, we present a graphical analysis of phase matching for typical conditions of our THG experiments with PCFs. The filled circles connected by a solid line display the spectrum of the third harmonic generated in a 30-cm piece of PCF by Cr:forsterite laser pulses with an input energy of 2 nJ and an initial pulse width of 120 fs. The central wavelengths of these peaks are virtually the same as the central wavelengths of the peaks observed in the spectrum of the third harmonic in Fig. 5. The spectral shapes of the peaks in these two figures are, however, slightly different because of different input pulse parameters. The solid lines labeled as dispersive waves in Fig. 6 represent the effective mode indices n_m of high-order PCF modes with field-intensity profiles shown in Fig. 2, calculated as functions of radiation wavelength in the third-harmonic spectral range, shown by the lower abscissa axis. The bold line shows the effective mode index n_{sol} of the soliton pump in the fundamental PCF mode as a function of the pump wavelength (the upper abscissa axis). Phase matching of Eq. (10) is achieved at the wavelengths λ where the bold line, representing $n_{\mathrm{sol}}(\lambda)$, crosses one of the solid lines, representing $n_m(\lambda/3)$.

The central frequencies of the peaks observed in the spectrum of the third harmonic, as can be seen from Fig. 6, correlate well with $n_{\mathrm{sol}}(\lambda)=n_m(\lambda/3)$ phase-matching resonances. The maximum THG conversion efficiency for a 40-cm PCF pumped by 2.5-nJ 100-fs Cr:forsterite laser pulses is on the order of 0.1% in our experiments. One of the possibilities for the improvement of the THG efficiency in PCFs involves designing PCFs with special dispersion and mode-area profiles providing larger interaction lengths for red-shifted solitons and the third-harmonic field. With appropriate dispersion and mode area profiles, the soliton frequency shift rate can be substantially reduced in the long-wavelength spectral region due to high-order dispersion effects and diffraction, allowing more efficient interaction of red-shifted solitons with third-harmonic pulses.

The presented experimental studies of the third-harmonic buildup in relation to the spectral evolution of the soliton pump field in a PCF provide the first direct experimental evidence of THG by a continuously red-shifting soliton pump. This regime of THG helps to identify new possibilities offered by nonlinear fiber optics and suggests attractive practical solutions for the creation of compact fiber-format light sources. The sequential generation of discrete spectral components in the third-harmonic region by a continuously frequency-shifting soliton allows the spectral content of the short-wavelength fiber output to be engineered by tailoring the frequency profiles of fiber dispersion and mode area, varying the input pulse parameters, and changing the fiber length. On the other hand, the third-harmonic PCF output with the spectrum shown in Fig. 5 holds much promise as a convenient fiber source for an ultrafast photoexcitation of a broad class of molecular systems in physics, chemistry, and biology.

To demonstrate this function of the considered regime of THG in PCFs, we chose solution of fluorescein dye as a test system. Absorption spectrum of fluorescein in solution is shown by curve 1 in Fig. 7. The fiber length and pulse parameters were optimized in these experiments to provide the maximum power of the peak at 445 nm. The spectrum of the third-harmonic output of this fiber scattered off a diffraction grating and filtered with a slit is presented by curve 2 in Fig. 7. The 445-nm peak in the third-harmonic output of the PCF, as can be seen from the comparison of curves 1 and 2 in Fig. 7, is ideally suited for the excitation of fluorescence in the dye solution. In experiments, this radiation was transmitted

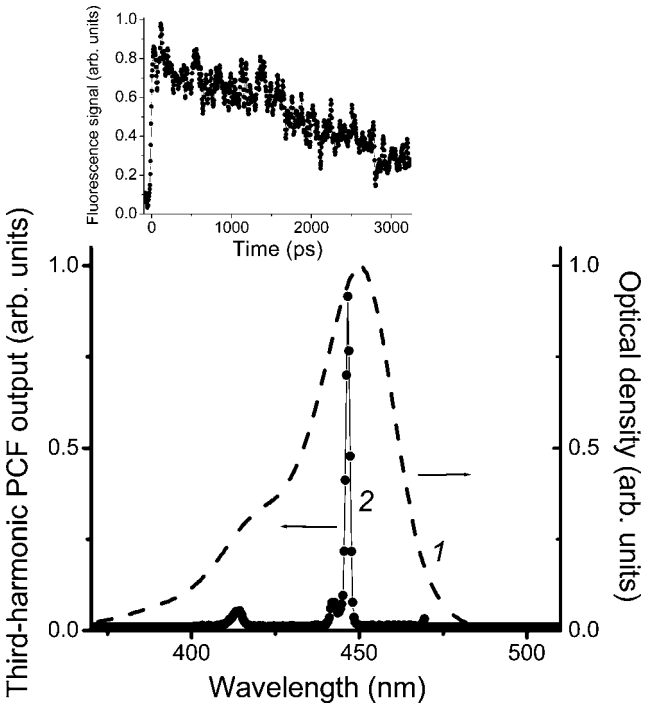

FIG. 7. Optical density of fluorescein dye solution (1) and the spectrum of the third-harmonic PCF output reflected off a diffraction grating and filtered with a slit (2). The inset shows the kinetics of the fluorescence signal of the dye excited by the third-harmonic output of the fiber.

through a 4-cm-thick cell with 50-nM fluorescein solution in ethanol, giving rise to a visible fluorescence signal. A typical kinetics of fluorescence excited by the 445-nm PCF output and measured by a streak camera with a 10-ps time resolution is presented in the inset to Fig. 7, indicating a standard nanosecond-scale fluorescence response time. The third-harmonic PCF output spectrum of Fig. 5 also perfectly fits the absorption spectra of green fluorescent protein and its variants, whose peak-absorption wavelengths range from 375 to 525 nm. This suggests an interesting application of the manifold of short-wavelength spectral components provided by the third-harmonic fiber output for the excitation of fluorescent proteins functioning as noninvasive fluorescent markers in living cells [44], including cell lineage tracers, reporters of gene expression, or indicators of protein-protein interactions.

IV. CONCLUSION

We have shown in this work that soliton regimes of pulse propagation in optical fibers and in PCFs, in particular, offer interesting new options for third-harmonic generation. Experiments presented here demonstrate that solitons excited in a PCF by unamplified femtosecond pulses of a Cr:forsterite laser can sweep through the spectral range from 1.25 to 1.65 μm, scanning through a manifold of THG phase-matching resonances with third-harmonic dispersive waves guided in PCF modes. THG optical nonlinearity and phase-matching resonances have thus been shown to map a continuous frequency shift of infrared solitons onto a set of intense, well-resolved third-harmonic peaks in the range of wavelengths from 370 to 550 nm at the output of the fiber, making PCF a compact fiber-format multifrequency source of short-wavelength radiation.

ACKNOWLEDGMENTS

We are grateful to K.V. Dukel'skii, A.V. Khokhlov, Yu. N. Kondrat'ev, and V. S. Shevandin for fabricating fiber samples. This study was supported in part by the Russian Foundation for Basic Research (Projects 06-02-16880 and 05-02-90566-NNS) and INTAS (Projects Nos. 03-51-5037 and 03-51-5288). The research described in this publication was made possible in part by Award No. RUP2-2695 of the U.S. Civilian Research & Development Foundation for the Independent States of the Former Soviet Union (CRDF).

[1] N. Bloembergen, *Nonlinear Optics* (Benjamin, New York, 1965).
[2] Y. R. Shen, *The Principles of Nonlinear Optics* (Wiley, New York, 1984).
[3] *Encyclopedia of Modern Optics*, edited by B. D. Guenther, D. G. Steel, and L. Bayvel (Elsevier, Amsterdam, 2005).
[4] A. H. Zewail, Science **242**, 1645 (1988).
[5] M. M. Fejer, G. A. Magel, D. H. Jundt, and R. L. Byer, IEEE J. Quantum Electron. **28**, 2631 (1992).
[6] P. St. J. Russell, Science **299**, 358 (2003).
[7] J. C. Knight, Nature (London) **424**, 847 (2003).
[8] J. K. Ranka, R. S. Windeler, and A. J. Stentz, Opt. Lett. **25**, 25 (2000).
[9] W. J. Wadsworth, A. Ortigosa-Blanch, J. C. Knight, T. A. Birks, T. P. M. Mann, and P. St. J. Russell, J. Opt. Soc. Am. B **19**, 2148 (2002).
[10] A. M. Zheltikov, J. Opt. A, Pure Appl. Opt. **8**, S47 (2006).
[11] W. H. Reeves, D. V. Skryabin, F. Biancalana, J. C. Knight, P. St. J. Russell, F. G. Omenetto, A. Efimov, and A. J. Taylor, Nature (London) **424**, 511 (2003).
[12] A. B. Fedotov, A. M. Zheltikov, A. P. Tarasevitch, and D. von der Linde, Appl. Phys. B **73**, 181 (2001).
[13] V. Finazzi, T. M. Monro, and D. J. Richardson, IEEE Photon. Technol. Lett. **15**, 1246 (2003).
[14] A. M. Zheltikov, Phys. Rev. A **72**, 043812 (2005).
[15] J. K. Ranka, R. S. Windeler, and A. J. Stentz, Opt. Lett. **25**, 796 (2000).
[16] F. G. Omenetto, A. Taylor, M. D. Moores, J. C. Knight, P. St. J. Russell, and J. Arriaga, Opt. Lett. **26**, 1558 (2001).
[17] F. G. Omenetto, A. Efimov, A. J. Taylor, J. C. Knight, W. J. Wadsworth, and P. St. J. Russell, Opt. Express **11**, 61 (2003).
[18] A. Efimov, A. J. Taylor, F. G. Omenetto, J. C. Knight, W. J. Wadsworth, and P. S. J. Russell, Opt. Express **11**, 910 (2003).
[19] A. Efimov, A. J. Taylor, F. G. Omenetto, J. C. Knight, W. J.

Wadsworth, and P. St. J. Russell, Opt. Express **11**, 2567 (2003).
[20] A. Efimov and A. J. Taylor, Appl. Phys. B **80**, 721 (2005).
[21] A. A. Ivanov, D. Lorenc, I. Bugar, F. Uherek, E. E. Serebryannikov, S. O. Konorov, M. V. Alfimov, D. Chorvat, and A. M. Zheltikov, Phys. Rev. E **73**, 016610 (2006).
[22] A. N. Naumov, A. B. Fedotov, A. M. Zheltikov, V. V. Yakovlev, L. A. Mel'nikov, V. I. Beloglazov, N. B. Skibina, and A. V. Shcherbakov, J. Opt. Soc. Am. B **19**, 2183 (2002).
[23] E. E. Serebryannikov, A. B. Fedotov, A. M. Zheltikov, A. A. Ivanov, M. V. Alfimov, V. I. Beloglazov, N. B. Skibina, D. V. Skryabin, A. V. Yulin, and J. C. Knight, J. Opt. Soc. Am. B (to be published).
[24] D. A. Akimov, A. A. Ivanov, A. N. Naumov, O. A. Kolevatova, M. V. Alfimov, T. A. Birks, W. J. Wadsworth, P. St. J. Russell, A. A. Podshivalov, and A. M. Zheltikov, Appl. Phys. B **76**, 515 (2003).
[25] S. Konorov, A. Ivanov, D. Ivanov, M. Alfimov, and A. Zheltikov, Opt. Express **13**, 5682 (2005).
[26] G. P. Agrawal, *Nonlinear Fiber Optics* (Academic Press, San Diego, CA, 2001).
[27] F. M. Mitschke and L. F. Mollenauer, Opt. Lett. **11**, 659 (1986).
[28] E. M. Dianov, A. Y. Karasik, P. V. Mamyshev, A. M. Prokhorov, V. N. Serkin, M. F. Stel'makh, and A. A. Fomichev, JETP Lett. **41**, 294 (1985).
[29] X. Liu, C. Xu, W. H. Knox, J. K. Chandalia, B. J. Eggleton, S. G. Kosinski, and R. S. Windeler, Opt. Lett. **26**, 358 (2001).
[30] H. N. Paulsen, K. M. Hilligsøe, J. Thøgersen, S. R. Keiding, and J. J. Larsen, Opt. Lett. **28**, 1123 (2003).
[31] D. A. Sidorov-Biryukov, E. E. Serebryannikov, and A. M. Zheltikov, Opt. Lett. **31**, 2323 (2006).
[32] A. M. Zheltikov, J. Opt. A, Pure Appl. Opt. **8**, S47 (2006).
[33] C. Y. Teisset, N. Ishii, T. Fuji, T. Metzger, S. Köhler, R. Holzwarth, A. Baltuska, A. M. Zheltikov, and F. Krausz, Opt. Express **13**, 6550 (2005).
[34] A. Yulin, D. V. Skryabin, and P. St. J. Russell, Opt. Lett. **29**, 2411 (2004).
[35] D. V. Skryabin and A. V. Yulin, Phys. Rev. E **72**, 016619 (2005).
[36] A. Efimov, A. J. Taylor, F. G. Omenetto, A. V. Yulin, N. Y. Joly, F. Biancalana, D. V. Skryabin, J. C. Knight, and P. St. J. Russell, Opt. Express **12**, 6498 (2004).
[37] K. J. Blow and D. Wood, IEEE J. Quantum Electron. **25**, 2665 (1989).
[38] E. E. Serebryannikov and A. M. Zheltikov, J. Opt. Soc. Am. B **23**, 1882 (2006).
[39] T. M. Monro, D. J. Richardson, N. G. R. Broderick, and P. J. Bennet, J. Lightwave Technol. **18**, 50 (2000).
[40] P. V. Mamyshev and S. V. Chernikov, Opt. Lett. **15**, 1076 (1990).
[41] B. Kibler, J. M. Dudley, and S. Coen, Appl. Phys. B **81**, 337 (2005).
[42] N. Akhmediev and M. Karlsson, Phys. Rev. A **51**, 2602 (1995).
[43] F. Biancalana, D. V. Skryabin, and A. V. Yulin, Phys. Rev. E **70**, 016615 (2004).
[44] M. Chalfie, Y. Tu, G. Euskirchen, W. W. Ward, and D. C. Prasher, Science **263**, 802 (1994).